

# An Optimal Electrical Impedance Tomography Drive Pattern for Human-Computer Interaction Applications

Gang Ma<sup>ID</sup>, Zhiliang Hao<sup>ID</sup>, Xuan Wu<sup>ID</sup>, and Xiaojie Wang<sup>ID</sup>

**Abstract**—In this article, we presented an optimal Electrical Impedance Tomography (EIT) drive pattern based on feature selection and model explanation, and proposed a portable EIT system for applications in human-computer interaction for gesture recognition and contact detection, which can reduce the measurement time and realize a performance trade-off between the accuracy and the time response. In our experiment, eleven hand gestures were designed to verify the proposed approach and EIT system. Compared to the traditional eight-electrode method, the optimal electrode drive pattern achieved a recognition accuracy of 97.5% with seven electrodes and the measurement time was reduced by 60%. To illustrate the universality of this method, we performed a contact detection experiment. By setting seven labels on the conductive panel and using optimal electrode drive pattern, the detection accuracy reached 100% with seven electrodes and the measurement time was reduced by 85%.

**Index Terms**—Contact detection, drive pattern, electrical impedance tomography (EIT), feature selection, gesture recognition, model explanation.

## I. INTRODUCTION

LECTRICAL impedance tomography (EIT) is an imaging technique that can detect the interior structural impedance distribution of a conductive object [1], [2]. By analyzing the impedance measurements from surface electrodes surrounding the subject, the inner impedance distribution can be monitored graphically in real-time. EIT technology has been mostly used for medical examination [3]–[6] and health monitoring of civil structures [7]–[9]. The advantages of this technology for detections lie in its radiation-free, non-destruction and fast response.

Manuscript received October 31, 2019; revised December 22, 2019 and January 10, 2020; accepted January 14, 2020. Date of publication January 20, 2020; date of current version May 27, 2020. This work was supported in part by Key Research and Development Plan of Jiangsu Province under Grant BE2017007-1, in part by Changzhou Applied Basic Research Program under Grant CJ20180016, in part by the Open Funding Project of National Key Laboratory of Human Factors Engineering under Grant 6142222190311, and in part by Changzhou Key Laboratory of high technology under Grant CM20183004. This paper was recommended by Associate Editor Prof. Nicole McFarlane. (*Corresponding author: Xiaojie Wang*.)

G. Ma is with the Department of Precision Machinery and Precision Instrumentation, University of Science and Technology of China, Hefei, Anhui 230026, China (e-mail: magang1209@foxmail.com).

Z. Hao, X. Wu, and X. Wang are with the Institute of Advanced Manufacturing Technology, Hefei Institutes of Physical Science, Chinese Academy of Sciences, Changzhou, Jiangsu 213164, China (e-mail: 374354691@qq.com; xwu@iamt.ac.cn; xjwang@iamt.ac.cn).

Color versions of one or more of the figures in this article are available online at <https://ieeexplore.ieee.org>.

Digital Object Identifier 10.1109/TBCAS.2020.2967785

As a tomography method, the image quality is crucial for practical applications. Many researchers have adapted various approaches to improve the resolution and accuracy of EIT images. The commonly used method is to increase the number of electrodes [10], [11] that enable more data to be generated for image reconstruction. It has been found that increasing the number of surface electrodes is salient for the quality of image; however, more electrodes cause practical problems in collecting data and placing electrodes [10]. In addition to adding the number of surface electrodes, some researchers suggested that inserting electrodes inside the conducting domain would improve the performance of EIT reconstructions [11]. However, this method is not suitable in practice that requires nondestructive and non-invasive operation especially for the medical application.

Another way to improve EIT image reconstruction is to enhance the diversity of measurement data through optimizing the drive patterns. To measure an unknown impedance, an excitation signal is required to alternately apply on the measured object through two surrounding electrodes, and simultaneously the response signals should be collected from the rest of the other surface electrodes. Therefore, choosing different electrode pairs for injecting and measuring will generate various drive patterns. Different driving patterns in EIT have been explored and implemented in the EIT system such as adjacent, opposite and cross drive patterns [12]–[14], etc. More complex driving patterns are also proposed and investigated. Adler *et al.* [15] tried to improve the adjacent drive pattern through adjusting the electrode placement. They suggested that the pair drive and measurement pattern separated by one electrode less than 180 degrees could achieve better results than that of most commonly used adjacent stimulation and measurement pattern. Hope *et al.* [16] studied several drive patterns for EIT imaging of neural activity in peripheral nerve, and built a finite element (FE) four-cylindrical shell model with two rings of 16 electrodes. Simulation results showed that longitudinal drive patterns are more robust against noise and errors for impedance reconstruction. However, all these efforts seek high resolution and accuracy of measurement at the cost of processing time.

Recently, the EIT technology has been emerging in the area of human-computer interaction (HCI) for robotic sensing and gesture recognition applications. An EIT-based tactile sensor for robotic sensing is described by [17], [18], which is flexible, stretchable, low-cost, and scalable. In this method, 16 electrodes were placed on the border of a rubberized and conductive

material that responded to pressure with local changes in conductivity. When the tactile sensor detected the applied pressure, EIT was employed to reconstruct the conductivity distribution. In order to improve the resolution of reconstructed image, Tawil *et al.* [11] described a multiple internal electrodes and optimized adjacent method by placing limited electrodes in the EIT-based tactile sensor. However, it brought the extra measurement and image reconstruction time. Yoon *et al.* [19] reported an EIT-based flexible sensor called iSoft, which utilized a dynamic baseline update process with 8 and 16 electrodes. It was shown that the EIT-based soft sensor could realize a real-time detections of fingertip contact and movement.

Since the electrical tomography is a nonlinear and severely ill-posed inverse problem [20], the traditional tomography approaches need to construct a Finite Element(FE) model of the system, resulting in high computational costs and deteriorated time resolution. Russo *et al.* [21] proposed to adapt supervised Machine Learning(ML) algorithms to EIT systems. They conducted an experiment of contact location identification by using opposite drive pattern with 8 and 16 electrodes and performed a test for the control of Kuka robot in real case scenarios by using recognition results. Results showed that this method realized a more accurate and faster recognition than traditional tomography approaches. Although they achieved some advantages by replacing traditional imaging algorithms with ML algorithms in EIT, they did not optimize the data acquisition mode [21]. Since the ML algorithm only requires some characteristic feature data rather than the whole impedance data, the traditional drive pattern combined with ML will cause data redundancy.

In the application of EIT technology in HCI, gesture recognition has attracted wide attention. It has been demonstrated that the bones and muscles within the wrist will show different status for various gestures that can be distinguished by interior impedance distribution. Therefore, the EIT technology can be employed to detect the impedance distribution, and consequently recognize the hand gestures. Zhang *et al.* [22] proposed a wearable armband sensor that combined with EIT and machine learning algorithms, named Tomo, which adopted two-terminal scheme measurement with eight electrodes to recognize eleven gestures, achieved an accuracy of 96.6%. Later, they upgraded Tomo [23], [24] by choosing more surface electrodes including 8, 16 and 32 electrodes and a more sophisticated four-terminal scheme measurement, concluding that more measurements can improve the image quality. However, the increase of measurements is at the cost of processing time and complex data acquisition. Wu *et al.* [25], [26] found the limitation of the hardware design in [22]–[24] and presented a high-performance EIT system using custom-made integrated circuit, which achieved an accuracy of 98% for gesture recognition in controlling hand prosthesis motion.

Although these methods achieved a high resolution and accuracy of reconstructed image, they resulted in tremendous measurement data and processing time. Since the gesture recognition as a classification problem only needs a subset of the original impedance data for classification rather than tomography process, which requires massive data to reconstruct the interior impedance distribution, we can develop a new drive pattern with less electrodes for a fast and accurate recognition.

Feature selection, as a main component of dimensionality reduction, plays a critical role in the machine learning for improving learning performance, preventing overfitting, and reducing computational costs [27]. By keeping a subset of the original features, a simpler and more comprehensive model can be built. When a model is built, understanding why the model makes a certain prediction can be as essential as its recognition accuracy [28]. Because knowing the relation between the output results and the input features can help us choose the most effective features and construct more robust model. In this study, we present a new drive pattern based on model explanation and feature selection, which can reduce the measurement time and achieve a performance trade-off between the accuracy and time response for real-time gesture recognition. Recursive feature elimination algorithm and SHAP (shapley additive explanations) values were used for feature selection and model explanation, respectively, so that the dimension of the data could be reduced. The optimal drive pattern is obtained through analyzing the simplified dataset. Five methods are used for data classification.

For a better demonstration and implementation of this method into practical devices, we employed two-terminal scheme in our EIT system. The strategy in the study is to firstly process and analyze the electrode signals from the EIT standard tests with eight-electrode mode, which are commonly used in the wearable hand gesture recognition systems. Then, we adopt feature selection and model explanation methods to get an optimal feature subset which has the characteristic of stable adaptability for the classification with satisfied accuracy. At last, the feature subset was mapped to the EIT drive pattern and the new drive pattern can avoid complicated measurement procedure, and reduce the number of surface electrodes. In the hand gesture recognition experiment, we designed eleven hand gestures to verify the proposed method. In addition, we performed a contact detection experiment to illustrate the universality of this method.

## II. SYSTEM DESIGN

The entire EIT system architecture is shown in Fig. 1. It consists of three parts: measurement scheme, data acquisition, data processing and classification. Firstly, the dimension of the impedance data is determined by choosing different drive pattern. Then, the impedance data of wrist is measured by homemade data acquisition system. Next, the collected data is sent to laptop for further data processing including feature selection, model explanation, training and recognition.

### A. Measurement Scheme

An EIT system can reconstruct the inner impedance distribution of a conductive object from the signals measured by surface electrodes. There are two most prevalent measurement strategies are shown in Fig. 2: two-terminal and four-terminal schemes [11], [29]. For the two-terminal scheme, only a pair of electrodes is selected to capture the impedance measurements. One of the electrodes acts as the emitter and the other serves as the receiver. We can get a round of electrical signal by replacing the measuring electrodes alternately with the remaining electrodes. However, this method will introduce contact impedance that affect imaging performance. The main reason

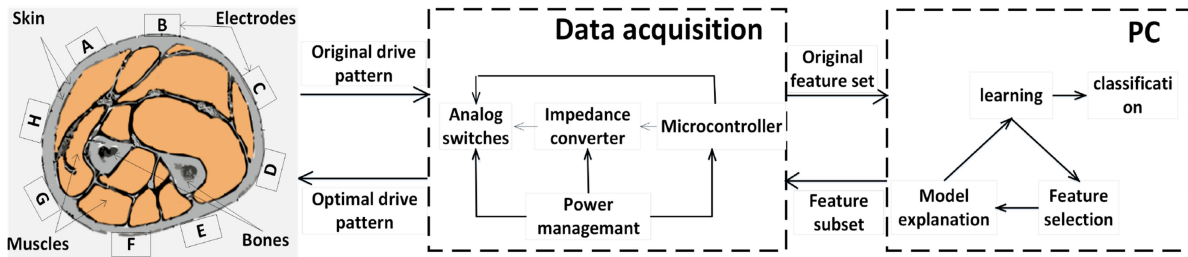


Fig. 1. The overall structures of the EIT system for classification.

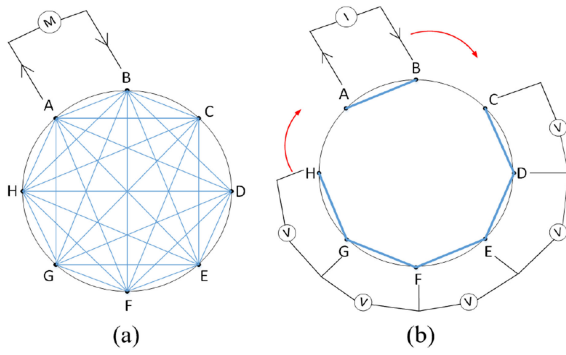


Fig. 2. Two drive patterns. (a) two-terminal scheme with eight electrodes. (b) four-terminal scheme with eight electrodes.

we chose two-terminal scheme is that this method requires less electrodes to complete impedance measurement and can reduce the complexity of hardware. Additionally, we are more interested in detecting the impedance changes rather than the absolute tissue impedance value as these changes provide information for sensing and gesture recognitions. The simple and cost-less system is appropriate for practical applications, especially for wearable devices. Regarding some disadvantages of the two-point impedance measurement in comparing with the four-point measurement scheme, such as the contact impedance and noise, we can remove the effect of the contact impedance by data preprocess. Compared with this pattern, the four terminal scheme is more sophisticated as it requires two pairs of electrodes to complete the measurement. Besides, choosing different pairs of electrodes as excitation and response can result in a series of complex drive patterns [15]. All these methods need to get as much as possible impedance data from all electrode pairs.

As mentioned above, EIT images have low spatial resolution due to limited number of independent measurements, the existing drive patterns of EIT are designed for imaging high spatial resolution EIT images rather than classification. However, gesture recognition only need a subset of the original impedance data for classification. Thus, we can seek for a new drive pattern that generates less impedance data for classification with sufficient accuracy. As two-terminal scheme requires less electrodes to complete impedance measurement that can reduce the complexity of hardware, and we can remove the effect of the contact impedance by data preprocess. In this study, we choose the most commonly used 8 electrodes and two-terminal scheme as benchmark for comparison.

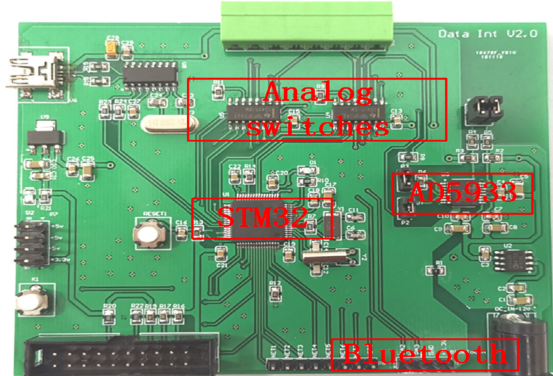


Fig. 3. The hardware. (top: data acquisition board; middle: medical electrodes with round shape (A-H); bottom: fixed electrodes around wrist.)

### B. Data Acquisition

We designed the data acquisition board (Fig. 3) based on an AD5933 Impedance Analyzer [30] and described the functional block diagram of the data acquisition board in Fig. 4. This chip includes a frequency generator and an on-board ADC that allow impedance measurement at a specific frequency range from 0 Hz to 100 KHz with a resolution of 0.1 Hz.

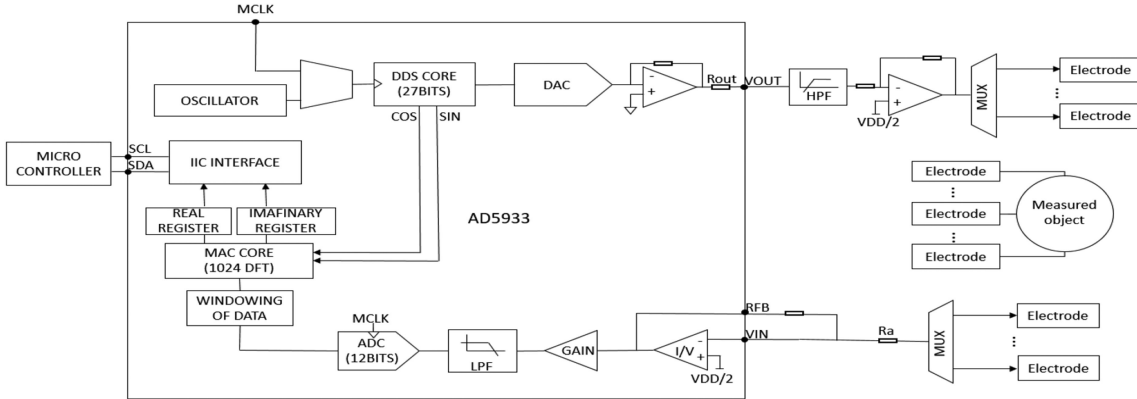


Fig. 4. Circuit schematic of the data acquisition board.

As shown in Fig. 4, the basic measurement process consists essentially of three parts: exciting the unknown impedance with a known voltage and a known frequency, then measuring the current flowing through the unknown impedance and computing its complex with discrete Fourier transform (DFT) algorithm. Although the AD5933 chip is a very useful integrated chip, it suffers from some drawbacks e.g. noise disturbance, dc bias, and safety issue [31], [32]. Takhti *et al.* [33] proposed a structured methodology for designing the main circuit building blocks of an EIT system and Hafid [32] proposed a method to adapt AD5933 to electrical bioimpedance (EBI) measurements. In order to limit the amount of ac current to conform to IEC 60601 standards (allowable ac current 400  $\mu$ A at 40 KHz) and remove the dc bias component that from the voltage output of AD5933, we introduced a precision resistor  $R_a$  3 k $\Omega$  and a high pass filter respectively. We used a constant excitation signal of 40 KHz that could realize a better recognition of different gestures [22]. The data acquisition board also includes two 8-to-1 analog switches (CD4051), which allow us to select any two of the electrodes as the emitter and the receiver. To distinguish different gestures, we should ensure that the surface electrodes are attached to the skin tightly and the contact impedance between skin and electrodes are consistent and stable for each test. Therefore, we selected the commercial medical electrodes which have been used for electromyography (EMG) signal measurement. In order to fit the wrist shape and reduce contact area, we tailored the commercial square electrodes into round electrodes. Since we are only interested in measuring the small impedance changes in the presence of the large contact impedance, in this study, we found that two electrodes attached to the wrist and a variable resistance that ranged from 0  $\Omega$  to 1 k $\Omega$  connected to our measurement board is acceptable for the measurement. In addition, the two electrodes can distinguish the impedance changes around the wrist for certain gestures. However, there are a few measured impedance have no significant change for some gestures.

The impedances between all electrodes pairs were measured sequentially without repetition, which resulted in 28 independent values (two-terminal scheme) and 40 independent values (four-terminal scheme). Then, the generated data was sent to laptop for imaging and classification.

### C. Data Processing and Classification

In this study, we only employed two-terminal scheme with eight electrodes to process the impedance analysis. There are 28 feature dimensions generated by this method. They have different weights in the classification models when making a prediction. Thus, a small feature subset can represent the original data. After collecting the data sets for different gestures, we divided them into two parts, one for training and the other for testing. We used five classification algorithms to train the original data for recognition. Feature selection approaches were used to reduce the dimensionality of data by selecting only a subset of measured features. Generally, feature selection can be grouped into three categories, i.e., filter, wrapper and embedded approaches [27], [31]. Filter approaches select features by ranking them with correlation coefficients. Wrapper approaches iteratively apply a heuristic search strategy to determine one or more small subsets of features and evaluate their corresponding performance of classification using an off-the-shelf classifier. Embedded approaches directly incorporate feature selection as a part of the classifier training process including decision trees, neural networks, lasso and robust feature selection. After analyzing each dimension of the original data to delete redundant and irrelevant features through feature selection, we got a small feature subset. The model explanation was applied to process the small feature subset and evaluate which features contribute to the prediction mostly. Next, the optimal feature subset was compared with the original impedance data by five classification models. Finally, the new drive pattern can be applied to our EIT system through mapping feature subset to electrode pairs.

## III. FEATURE SUBSET

### A. Gesture Sets

We designed eleven hand gestures combining most features of previous work [22]–[26] for comparison. The gesture set included Spider-Man, Index Pinch, Middle Pinch, Left, Right, Fist, Thumbs Up, Scratch, Relax, Fire and Stretch (Fig. 5).

There are five participants with a mean age of 22 in the process of collecting gesture datasets. Before the measurement tests,

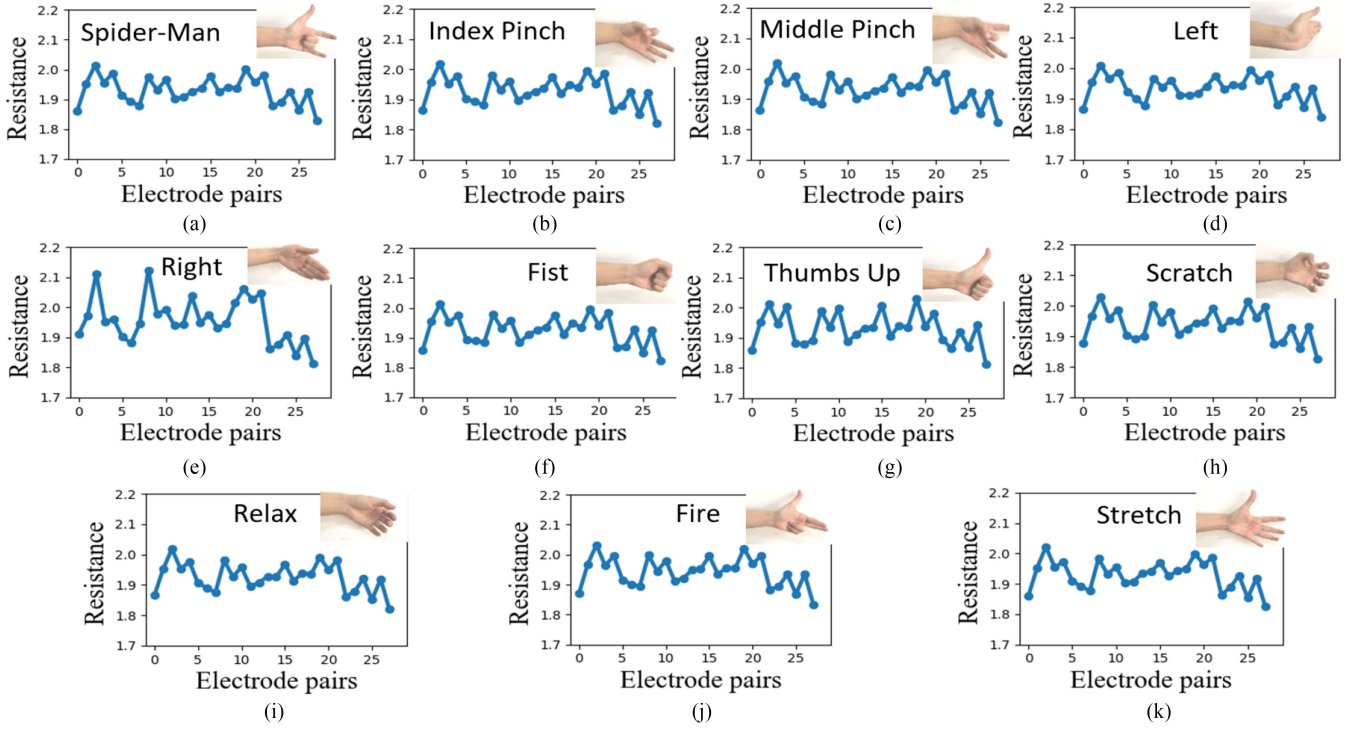


Fig. 5. Eleven hand gestures and the impedance data of distribution: (a)–(k).

the wrist was cleaned with medical alcohol and the participant maintained a comfortable sitting posture. Then eight electrodes were evenly attached to the wrist. Next, the participant practiced 11 designed gestures for a while. During the testing, a laptop was used to start and end of data collection. Twenty testing samples for each designed gesture were recorded by the laptop. In every 10 seconds, different gesture measurement was carried out until all 11 gestures had been done. Five repeated cycles were performed for each participant. One of the cycles is used as a testing set, and the other four are used as training sets. The whole experiment took approximately three hours, and there's a total of 5500 samples were acquired.

### B. Feature Selection

The Fig. 6 shows the software flow diagram of the system. Considering that there may be some ambient noise when collecting the impedance data, the threshold filtering and average filtering methods were applied to preprocess these data. Additionally, the normalization method was adapted to preprocess these data to remove the effect of the contact impedance. Then a five-fold cross-validation was adapted to our datasets as the data collection included 5 cycles. Next, we selected five common classification models for hand gesture recognition including Support Vector Machine (SVM), Random Forest (RF), K-Nearest Neighbor (KNN), Logistic Regression (LR) and Adaboost. Table I shows the recognition accuracy of these five algorithms on the original impedance data  $X_0$ . As we can see, the Adaboost achieves the highest accuracy of 98.11%. However, it may take more time to process the data for recognition. The

TABLE I  
RECOGNITION ACCURACY AND TRAINING TIME WITH ORIGINAL DRIVE PATTERN

Algorithms	Accuracy (%)	Training Time (s)
SVM	97.32	0.47
RF	97.61	1.43
KNN	95.08	0.68
LR	96.86	8.64
Adaboost	98.11	1.64

reason lies in a fact that the original data has 28 feature dimensions that need collect more data to complete each recognition. In order to reduce the measurement time and keep an acceptable accuracy, we need to find a feature subset of the original data. First, we computed the variance of each dimension in the original data and set the threshold to mark insensitive features, and then use the Pearson Correlation to filter these linear features. Next, RFE (Recursive feature elimination) [35] algorithm is used to repeatedly construct the classification model and remove the features with low weight coefficient. Fig. 7 shows the relation between the number of features and the cross validations scores. When the number of features is fourteen, the model could get the highest score of accuracy, which indicates that we can reduce the dimension of data without losing too much accuracy. As these impedance data were collected from the electrode pairs and the name of the features were recorded according to the measurement index, a map between features and electrode pairs were established. Mapping the selected features to the original impedance data, we can get a simplified drive pattern whose electrode pairs merely including AB, AG, BC, BD, BF, CD, CG,

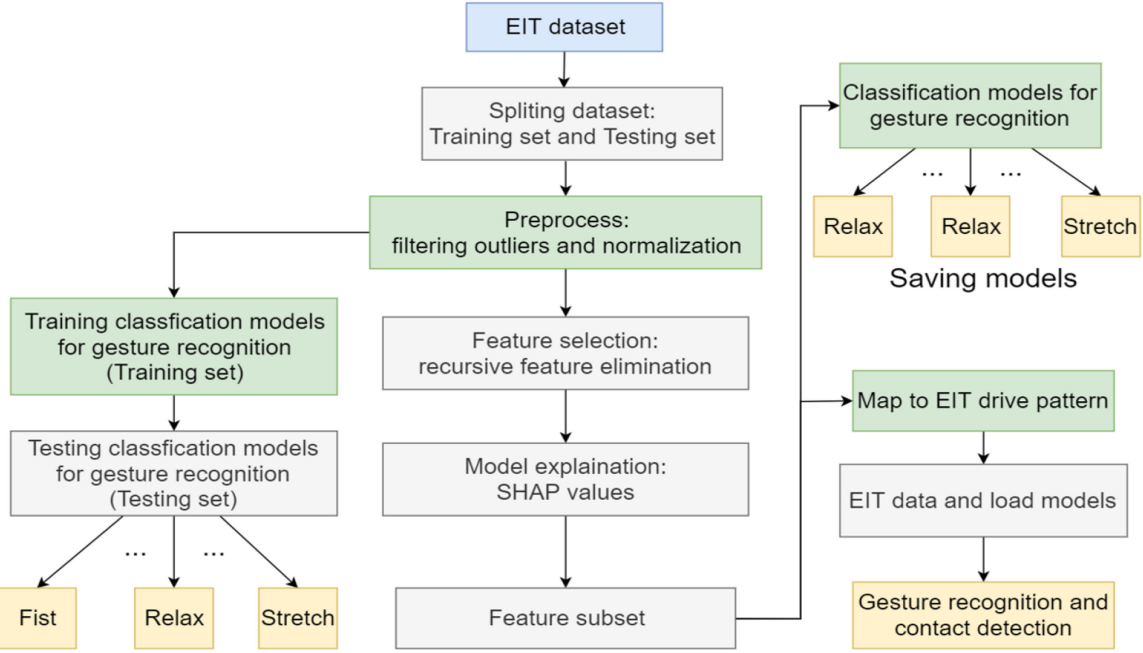


Fig. 6. Software flow diagram of the system for gesture recognition and contact detection.

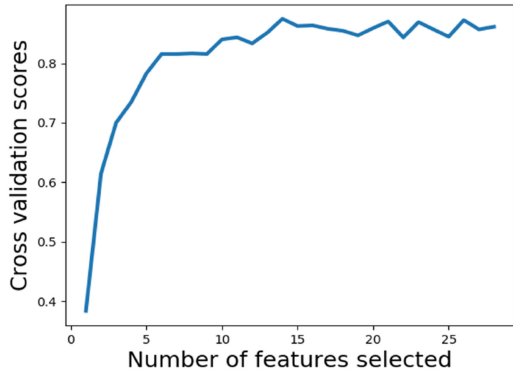


Fig. 7. Relation between the number of features and model scores.

DE, DF, DG, EF, EG, FH, GH. Compared with original drive pattern, feature selection has helped us to reduce 50% electrode pairs that means 50% measurement time was saved.

### C. Model Explanation

After feature selection, we can get a simplified dataset that has a feature dimension of fourteen. In order to find an optimal feature subset, model explanation method was used to help us to understand the relation between features and the classification models. Therefore, we adopted SHAP (Shapley additive explanations) values [36] to explain the models, which is a measurement of the feature characteristics through calculating the impact of each feature on the change in model prediction.

As proposed in [28], we focus on local methods, which identify an interpretable model over the interpretable representation that is locally faithful to the classifier. The best explanation of a

simple model is the model itself. However, it is often impossible for an explanation to be completely faithful as it's not complete description of the model itself. For an explanation to be meaningful it must at least be locally faithful, i.e. it must correspond to how the model behaves in the vicinity of the instance being predicted. Let  $f$  and  $g \in G$  respectively represent prediction model and explanation model, where  $G$  is a class of potentially interpretable models, such as linear models, decisions trees. A model  $g$  can be readily presented to the user. Interpretable representation should be understandable to humans, regardless of the actual features used by the model. We denote  $x \in R^d$  be the original feature, and we use  $x' \in \{0, 1\}^{d'}$  to denote a binary vector for its interpretable representation. Then, through a mapping function  $x = h_x(x')$  map simplified features  $x'$  to  $x$ , and ensure  $g(z') \approx f(h_x(z'))$  whenever  $z' \approx x'(z' \in \{0, 1\}^M)$ ,  $M$  is the number of simplified features. Next, we get the additive feature attribution methods with an explanation model in Equation (1) and the Shapley values [34] for computing explanations of model predictions in Equation (2):

$$f(h_x(z')) \approx g(z') = \phi_0 + \sum_{i=1}^M \phi_i z'_i \quad (1)$$

$$\phi_i(f, x) = \sum_{z' \subseteq x'} \frac{|z'|!(M - |z'| - 1)!}{M!} [f_x(z') - f_x(z' \setminus i)] \quad (2)$$

Equation (1) attributes an effect  $\phi_i$  to each feature, Equation (2) follows from combined cooperative game theory results, where the values  $\phi_i$  are known as Shapley values, and  $|z'| = \sum_{i=1}^M z'_i$ . SHAP values are the Shapley values of a conditional expectation function of the original model, thus, we can get the solution of Equation (2) in Equation (3) (note that  $S$  is the set

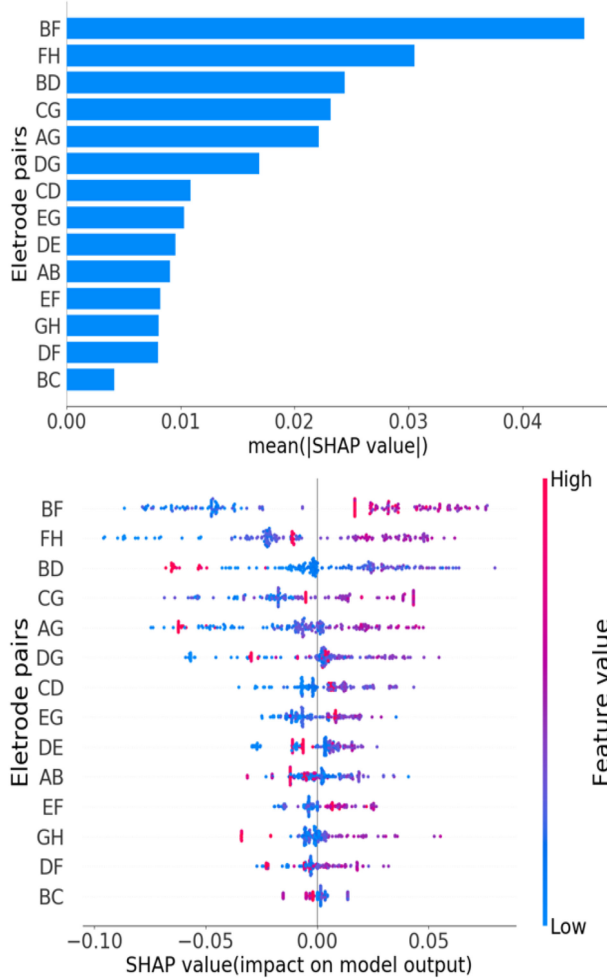


Fig. 8. Top: Mean SHAP values of features. Bottom: The impact of features value on the model.

of non-zero indexes in  $z'$  and  $\bar{S}$  is the set of features not in  $S$ ).

$$f(h_x(z')) = E[f(z)|z_S] = E_{z_{\bar{S}}|z_S}[f(z)] \quad (3)$$

It's arduous to compute the SHAP values. Consequently, additive feature attribution methods combined with two assumptions was used to get an approximation.

$$f(h_x(z')) \approx E_{z_{\bar{S}}}[f(z)] \quad \text{Assume feature independence} \quad (4)$$

$$\approx f([z_S, E[z_{\bar{S}}]]) \quad \text{Assume model linearity} \quad (5)$$

Fig. 8 shows the relation between features and model prediction. As shown in Fig. 8 (top), the features present different values for different electrode pairs according to their contribution to the model prediction. The electrode pairs BF, FH, BD, CG, AG, and DG contribute most to the model prediction. Fig. 8(bottom) describes the impact on model output with the change of feature value in more detail. For each point in the figure, the vertical coordinate tells us which feature it belongs to, the color represents the numerical size, and the horizontal coordinate shows the impact on model output. From these

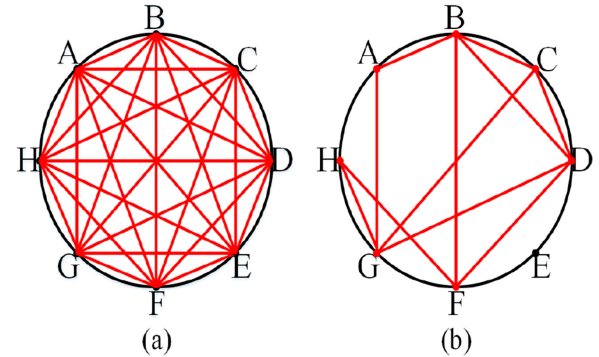


Fig. 9. Two different drive patterns (red lines represent electrode pairs for measurement): (a) original drive pattern (b) new drive pattern.

points, we can not only get that different features have various contribution to model output, but also know how the change of a certain feature value impact on model output. As we can see, the top features in Fig. 8 (top) have a great impact on model prediction and the electrode pairs EG, DE, EF contribute less to the model prediction. Additionally, these top features share a common character that they have nothing to do with electrode E. Therefore, filtering these electrode pairs would have minimum effect on our recognition system while bring a big benefit for reducing the number of electrodes as well as the dimension of the features. Finally, we can get the feature subset  $X_2$  ( $X_2 \subseteq X_1$ ), which has the feature dimension of eleven.

#### IV. RESULTS

In this section, the results of the new drive pattern and original drive will be presented and their difference will be discussed. At last, the advantages of the proposed method will be shown by two experiments: one is the real-time gesture recognition, which will demonstrate the effectiveness of the new drive pattern; the other is a contact detection experiment that is designed to verify the universality of this new method in EIT applications.

##### A. Optimal Drive Pattern

New drive pattern was obtained by mapping the feature subset to electrode pairs of measurement. As can be seen in Fig. 9(a), the original drive pattern needs eight electrodes A-H and takes twenty eight measurement times to perform one measure, which brings data redundancy and extra cost of time. Compared with the original drive pattern, our new drive pattern (Fig. 9(b)) only need eleven measurements for a cycle, which saves 60% measurement time. In addition, our new drive pattern can be reduced to seven electrodes for classification. Table II shows the recognition accuracy and training time of optimal drive pattern with original drive pattern by five classification algorithms. The results show that as the electrode pairs reduced, the accuracy loss is various from 0.6% to 8%. The ensemble methods of RF and Adaboost with seven electrodes can achieve the same accuracy as that of the original drive pattern with eight electrodes.

TABLE II  
THE ACCURACY VALUES AND TRAINING TIME OF ELEVEN HAND GESTURES  
FOR ORIGINAL DRIVE PATTERNS

Algorithms	Accuracy (%)	Training Time (s)
SVM	97.32	0.35
RF	97.61	1.21
KNN	95.08	0.57
LR	96.86	5.23
Adaboost	98.11	1.37



Fig. 10. Real-time gesture recognition with new drive pattern.

### B. Real-Time Gesture Recognition

The proposed method for real time interactive control were carried out on the EIT based gesture recognition system. The recognition results are shown in Fig. 10. As can be seen, when we make a gesture of thumbs up, the EIT system with new drive pattern will acquire the impedance data and send it to the laptop. Simultaneously, the gesture is shown on the screen of the laptop. As we change the gestures, the laptop will display different gesture pictures to complete an instant interaction. The experimental results indicate that the illustrated new drive pattern can not only simplify the EIT system by using less electrodes, but also reduce the measurement time, which verifies the effectiveness of this proposed method (S video 1).

### C. Real-Time Contact Detection

In order to illustrate the universality of this method, a contact detection experiment was performed rather than hand gesture recognition. We sprayed the conductive paint evenly on an A4 paper to obtain a conductive plate (Fig. 11(a)), and the electrodes were placed evenly around the conductive plate. When we touch different positions of the conductive plate, it will have different impedance distribution. Based on these differences, the model can recognize the contact position immediately. As illustrated in Fig. 11(b), we selected eight state including no touch and seven touch positions (1–7) as our recognition target. When a conductive coin whose diameter is 25 mm was put on any position of these seven positions, we can quickly get its position from our EIT system.

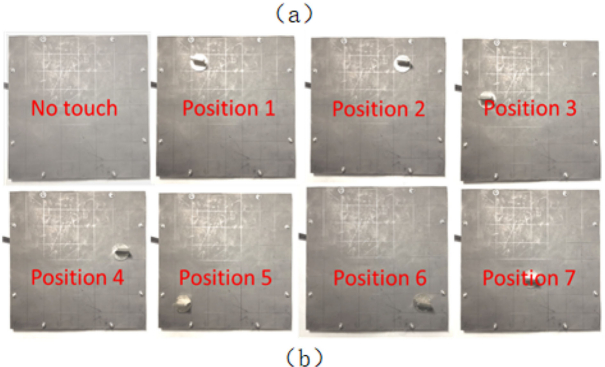
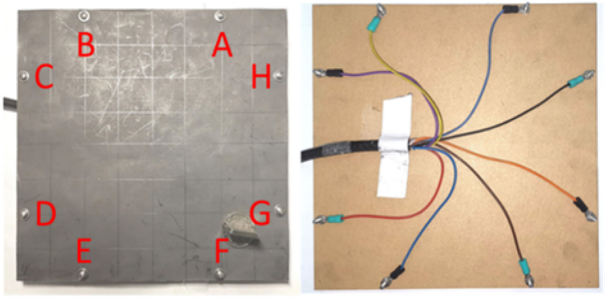


Fig. 11. (a) conductive plate with eight electrodes (A-H), eight silver electrodes were placed evenly on the plate surface. (b): Putting the coin on the different positions to generate eight target.

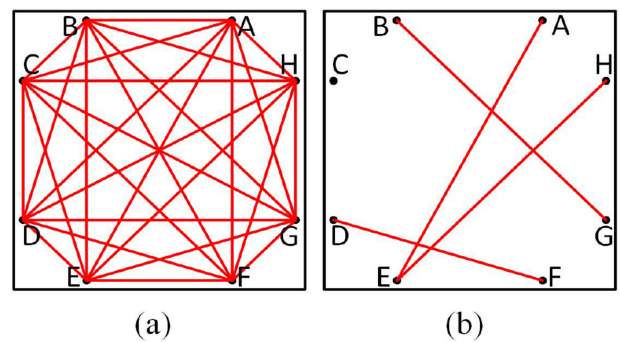


Fig. 12. Two different drive patterns: (a) original drive pattern(eight electrodes) need twenty eight measurement times (b) new drive pattern (seven electrodes) need four measurement times.

At first, we use the original drive pattern with eight electrodes to collect original datasets. As shown in Fig. 12(a), it need twenty eight measurement times to complete one measure. After collecting datasets, we do the same work as in gesture recognition experiment, then we can get the optimal drive pattern in Fig. 12(b) and the feature subset from our original datasets. As Fig. 12(b) shows, we can greatly improve the EIT efficiency as the measurement time reduces up to 85%, while achieving an accuracy 100% Table III with seven electrodes (without C). Compared with the previous work of gesture recognition, the contact detection by using the new method is more effective in sensing position. The reason may be due to the impedance distribution of the conductive plate is not as complicated as the human body. Next, according to the feature subset, we

TABLE III  
ACCURACIES FOR SEVEN TOUCH POSITION ACROSS TWO DIFFERENT DRIVE PATTERNS (ORIGINAL: ORIGINAL DRIVE PATTERN, OPTIMAL: NEW DRIVE PATTERN)

Algorithms	Original (%)	Optimal (%)
SVM	100	100
RF	100	100
KNN	100	99.74
LR	98.99	97.47
Adaboost	100	100

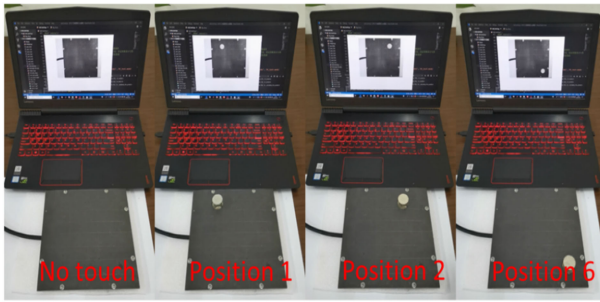


Fig. 13. Real-time detection with optimal drive pattern (seven electrodes without C), the laptop shows the recognition result on the screen, and a gray circle is used to point out the contact position on the screen.

implemented the new drive pattern to the EIT-based sensing system and showed the results of real-time contact detection.

Fig. 13 shows some results of contact detection with new drive pattern (details in S video 2). As can be seen, the EIT system achieved a real-time contact detection with seven electrodes (without electrode C). When the coin had no contact with conductive plate, the laptop would recognize the state of the plate and displayed a blank picture on the screen. As the coin was put on the plate, and changed its position, the screen would show the coin position by a gray circle on the blank picture instantly. In this trial, our EIT system realized a real-time contact detection with only seven electrodes by using the proposed method, which demonstrates the universality of the new EIT drive pattern.

## V. CONCLUSION

We designed an EIT system for hand gesture recognition and proposed a drive pattern for EIT classification based on feature selection and model explanation. The new method significantly saves the measurement time and reduces electrodes for classification that can be used for effective gesture recognition. In order to verify the universality of this approach, we applied the method on a contact detection experiment. Our results demonstrated that the proposed method is effective and universal. However, the experimental validation was carried out only for static gesture tests because of the hardware limitation in the data acquisition. In the future, we will upgrade our EIT system and explore more possibilities for dynamic gesture recognition.

## REFERENCES

- [1] R. P. Henderson and J. G. Webster, "An impedance camera for spatially specific measurements of the thorax," *IEEE Trans. Biomed. Eng.*, vol. BME-25, no. 3, pp. 250–254, May 1978.
- [2] R. H. Bayford, "Bioimpedance tomography (electrical impedance tomography)," *Annu. Rev. Biomed. Eng.*, vol. 8, pp. 63–91, 2006.
- [3] A. Adler *et al.*, "GREIT: A unified approach to 2 d linear EIT reconstruction of lung images," *Physiol. Meas.*, vol. 30, no. 6, 2009, Art. no. S35.
- [4] R. Harikumar, R. Prabu, and S. Raghavan, "Electrical impedance tomography (EIT) and its medical applications: A review," *Int. J. Soft Comput. Eng.*, vol. 3, no. 4, pp. 193–198, 2013.
- [5] T. Dowrick, C. Blochet, and D. Holder, "In vivo bioimpedance measurement of healthy and ischaemic rat brain: Implications for stroke imaging using electrical impedance tomography," *Physiol. Meas.*, vol. 36, no. 6, 2015, Art. no. 1273.
- [6] C. J. Roth, T. Becher, I. Frerichs, N. Weiler, and W. A. Wall, "Coupling of EIT with computational lung modeling for predicting patient-specific ventilatory responses," *J. Appl. Physiol.*, vol. 122, no. 4, pp. 855–867, 2016.
- [7] T. Rymarczyk, P. Adamkiewicz, K. Duda, J. Szumowski, and J. Sikora, "New electrical tomographic method to determine dampness in historical buildings," *Arch. Elect. Eng.*, vol. 65, no. 2, pp. 273–283, 2016.
- [8] T. Rymarczyk, G. Kłosowski, and E. Kozłowski, "A non-destructive system based on electrical tomography and machine learning to analyze the moisture of buildings," *Sensors*, vol. 18, no. 7, 2018, Art. no. 2285.
- [9] D. Smyl, M. Pour-Ghaz, and A. Seppänen, "Detection and reconstruction of complex structural cracking patterns with electrical imaging," *NDT & E Int.*, vol. 99, pp. 123–133, 2018.
- [10] M. Tang, W. Wang, J. Wheeler, M. McCormick, and X. Dong, "The number of electrodes and basis functions in EIT image reconstruction," *Physiol. Meas.*, vol. 23, no. 1, pp. 129–140, 2002.
- [11] D. S. Tawil, D. Rye, and M. Velonaki, "Improved image reconstruction for an EIT-based sensitive skin with multiple internal electrodes," *IEEE Trans. Robot.*, vol. 27, no. 3, pp. 425–435, Jun. 2011.
- [12] B. H. Brown and A. D. Seagar, "The Sheffield data collection system," *Clin. Phys. Physiol. Meas.*, vol. 8, no. 4 A, pp. 91–97, 1987.
- [13] N. Avis and D. Barber, "Image reconstruction using non-adjacent drive configurations (electric impedance tomography)," *Physiol. Meas.*, vol. 15, no. 2 A, pp. A153–A160, 1994.
- [14] X. Shi, X. Dong, W. Shuai, F. You, F. Fu, and R. Liu, "Pseudo-polar drive patterns for brain electrical impedance tomography," *Physiol. Meas.*, vol. 27, no. 11, pp. 1071–1080, 2006.
- [15] A. Adler, P. O. Gaggero, and Y. Maimaitijiang, "Adjacent stimulation and measurement patterns considered harmful," *Physiol. Meas.*, vol. 32, no. 7, pp. 731–744, 2011.
- [16] J. Hope, F. Vanholsbeeck, and A. McDaid, "Drive and measurement electrode patterns for electrode impedance tomography (EIT) imaging of neural activity in peripheral nerve," *Biomed. Phys. Eng. Express*, vol. 4, no. 6, 2018, Art. no. 067002.
- [17] A. Nagakubo, H. Alirezaei, and Y. Kuniyoshi, "A deformable and deformation sensitive tactile distribution sensor," in *Proc. IEEE Int. Conf. Robot. Biomimetics*. 2007, pp. 1301–1308.
- [18] Y. Kato and T. Mukai, "Tactile sensor without wire and sensing element in the tactile region using new rubber material," *Sensors, Focus Tactile, Force, Stress Sensors*, pp. 399–408, 2008.
- [19] S. H. Yoon *et al.*, "iSoft: A customizable soft sensor with real-time continuous contact and stretching sensing," in *Proc. 30th Annu. ACM Symp. User Interface Softw. Technol.*, 2017, pp. 665–678.
- [20] D. Silvera-Tawil, D. Rye, M. Soleimani, and M. Velonaki, "Electrical impedance tomography for artificial sensitive robotic skin: A review," *IEEE Sensors J.*, vol. 15, no. 4, pp. 2001–2016, Apr. 2015.
- [21] S. Russo, R. Assaf, N. Carbonaro, and A. Tognetti, "Touch position detection in electrical tomography tactile sensors through quadratic classifier," *IEEE Sensors J.*, vol. 19, no. 2, pp. 474–483, Jan. 2019.
- [22] Y. Zhang and C. Harrison, "Tomo: Wearable, low-cost electrical impedance tomography for hand gesture recognition," in *Proc. 28th Annu. ACM Symp. User Interface Softw. Technol.*, 2015, pp. 167–173.
- [23] Y. Zhang, R. Xiao, and C. Harrison, "Advancing hand gesture recognition with high resolution electrical impedance tomography," in *Proc. 29th Annu. Symp. User Interface Softw. Technol.* ACM, 2016, pp. 843–850.
- [24] Y. Zhang, G. Laput, and C. Harrison, "Electrick: Low-cost touch sensing using electric field tomography," in *Proc. CHI Conf. Human Factors Comput. Syst.* ACM, 2017, pp. 1–14.
- [25] Y. Wu, D. Jiang, J. Duan, X. Liu, R. Bayford, and A. Demosthenous, "Towards a high accuracy wearable hand gesture recognition system using EIT," in *Proc. IEEE Int. Symp. Circuits Syst.* 2018, pp. 1–4.
- [26] Y. Wu, D. Jiang, X. Liu, R. Bayford, and A. Demosthenous, "A human-machine interface using electrical impedance tomography for hand prosthesis control," *IEEE Trans. Biomed. Circuits Syst.*, vol. 12, no. 6, pp. 1322–1333, Dec. 2018.

- [27] J. Li *et al.*, "Feature selection: A data perspective," *ACM Comput. Surv.*, vol. 50, no. 6, 2018, Art. no. 94.
- [28] M. T. Ribeiro, S. Singh, and C. Guestrin, "Why should I trust you?: Explaining the predictions of any classifier," in *Proc. 22nd ACM SIGKDD Int. Conf. Knowl. Discovery Data Mining*. ACM, 2016, pp. 1135–1144.
- [29] A. McEwan, G. Cusick, and D. Holder, "A review of errors in multi-frequency EIT instrumentation," *Physiol. Meas.*, vol. 28, no. 7, 2007, Art. no. S197.
- [30] Analog Devices, "Ad5933 datasheet," 2007. [Online]. Available: <http://www.analog.com/static/imported-files/datasheets/AD5933.pdf>
- [31] F. Seoane, J. Ferreira, J. J. Sanchez, and R. Bragós, "An analog front-end enables electrical impedance spectroscopy system on-chip for biomedical applications," *Physiol. Meas.*, vol. 29, no. 6, 2008, Art. no. S267.
- [32] A. Hafid, S. Benouar, M. Kedir-Talha, F. Abtahi, M. Attari, and F. Seoane, "Full impedance cardiography measurement device using raspberry PI3 and system-on-chip biomedical instrumentation solutions," *IEEE J. Biomed. Health Inform.*, vol. 22, no. 6, pp. 1883–1894, 2017.
- [33] M. Takhti and K. Odame, "Structured design methodology to achieve a high SNR electrical impedance tomography," *IEEE Trans. Biomed. Circuits Syst.*, vol. 13, no. 2, pp. 364–375, Apr. 2019.
- [34] J. Gui, Z. Sun, S. Ji, D. Tao, and T. Tan, "Feature selection based on structured sparsity: A comprehensive study," *IEEE Trans. Neural Netw. Learn. Syst.*, vol. 28, no. 7, pp. 1490–1507, Jul. 2017.
- [35] Q. Chen, Z. Meng, X. Liu, Q. Jin, and R. Su, "Decision variants for the automatic determination of optimal feature subset in RF-RFE," *Genes*, vol. 9, no. 6, 2018, Art. no. 301.
- [36] S. M. Lundberg and S.-I. Lee, "A unified approach to interpreting model predictions," in *Proc. Adv. Neural Inf. Process. Syst.*, 2017, pp. 4765–4774.
- [37] L. S. Shapley, "A value for n-person games," *Contributions Theory Games*, vol. 2, no. 28, pp. 307–317, 1953.



**Gang Ma** received the B.S. degree in electrical engineering from Zhengzhou University, Zhengzhou, China, in 2015. He is currently working toward the Ph.D. degree with the Department of Precision Machinery and Precision Instrumentation, University of Science and Technology of China, Hefei, China and doing research on EIT based gesture recognition system at the Bioinspired Robotics and Intelligent Material Laboratory, Institute of Advanced Manufacturing Technology, Chinese Academy of Sciences. His research interests include biomedical image/signal processing, electrical impedance tomography and machine learning.



**Zhiliang Hao** received the B.S. degree in electrical engineering from Anhui University, Anhui, China, and the M.S. degree in Control engineering from the Chongqing University of Posts and Telecommunications, Chongqing, China, in 2016 and 2019, respectively. From 2017 to 2019, he joined the Bio-inspired Robotics and Intelligent Material Laboratory, Institute of Advanced Manufacturing Technology, where he was a visiting student. He is currently working with Huawei Technologies Co., Ltd., Shenzhen, China for Linux device driver development and network device driver programming.



**Xuan Wu** received the B.Eng. and Ph.D. degrees from the University of Science and Technology of China, Hefei, China, in 2009 and 2015, respectively. He joined the Bio-inspired Robotics and Intelligent Material Laboratory, Institute of Advanced Manufacturing Technology, Hefei Institutes of Physical Science in 2015, and is currently an Associate Professor. His research interests include bioinspired robotics.



**Xiaojie Wang** received the B.S. degree in fluid mechanics from Tsinghua University, Beijing, China, in 1989, the M.S. degree in solid mechanics from the University of Science and Technology of China, Hefei, China, in 1998, and the Ph.D. degree from the Department of Mechanical Engineering, University of Nevada, Reno, NV, USA, in 2002. Dr. Wang is the Founder and Director of the Bio-inspired Robotics and Intelligent Material Laboratory, Institute of Advanced Manufacturing Technology, Chinese Academy of Sciences, Beijing, China. He is an Adjunct Professor with the University of Science and Technology of China, Hefei, China, and also serves as External Supervisor in the Faculty of Engineering and Information Technology, University of Technology Sydney, Australia. Prior to joining the CAS, he had been conducting research on intelligent materials and devices at University of Nevada, Reno for more than 10 years. He is author/coauthor of more than 150 scientific publications with chapters in three books and holds six patents. His research interests are in the areas of bio-inspired robots, smart materials, sensor/actuator and mechatronic systems.